Tellus **000**, 000–000 (0000) Printed 13 April 2010 (Tellus LaTeX style file v2.2)

Probabilistic hindcasts and projections of the coupled climate, carbon cycle, and Atlantic meridional overturning circulation system: A Bayesian fusion of century-scale observations with a simple model

By NATHAN M. URBAN[1⋆] and KLAUS KELLER[1,2],
[1] *Department of Geosciences, Penn State University, University Park, PA 16802, U.S.A.*
[2] *Earth and Environmental Systems Institute, Penn State University, University Park, PA 16802, U.S.A.*

13 April 2010

ABSTRACT

How has the Atlantic Meridional Overturning Circulation (AMOC) varied over the past centuries and what is the risk of an anthropogenic AMOC collapse? We report probabilistic projections of the future climate which improve on previous AMOC projection studies by (i) greatly expanding the considered observational constraints and (ii) carefully sampling the tail areas of the parameter probability distribution function (pdf). We use a Bayesian inversion to constrain a simple model of the coupled climate, carbon cycle, and AMOC systems using observations to derive multi-century hindcasts and projections.

Our hindcasts show considerable skill in representing the observational constraints. We show that robust AMOC risk estimates can require carefully sampling the parameter pdfs. We find a low probability of experiencing an AMOC collapse within the 21st century for a business-as-usual emissions scenario. The probability of experiencing an AMOC collapse within two centuries is 1/10. The probability of crossing a forcing threshold and triggering a future AMOC collapse (by 2300) is approximately 1/30 in the 21st century and over 1/3 in the 22nd. Given the simplicity of the model structure and uncertainty in the forcing assumptions, our analysis should be considered a proof of concept and the quantitative conclusions subject to severe caveats.

1 Introduction

Fossil fuel consumption has driven atmospheric carbon dioxide (CO_2) concentrations far beyond the range experienced by previous civilizations. This anthropogenic perturbation of the Earth system has already committed future generations to considerable climate change, with potentially profound and irreversible effects on ecosystems and human society (Adger et al., 2007; Alley et al., 2007). Here we focus on a key example of such an anthropogenic climate change impact: a potential collapse of the Atlantic meridional overturning circulation (AMOC) (Stouffer et al., 2006). An AMOC collapse would likely have nontrivial economic impacts, for example by changes in global temperature and precipitation patterns (Keller et al., 2000; 2004; Link and Tol, 2004; Vellinga and Wood, 2002; Schneider et al., 2007a; Kuhlbrodt et al., 2009).

The AMOC is sensitive to anthropogenic climate forcings (Meehl et al., 2007, Sec. 10.3.4). Current surface temperature patterns are strongly influenced by the Gulf stream and the North Atlantic current (Vellinga and Wood, 2002). These surface currents transport heat from the tropics to higher northern latitudes in the Atlantic basin. The heat loss from the surface waters to the atmosphere cools the waters and acts to increase the water density. In addition, the formation of sea ice at high latitudes acts to increase the salinity of the surface waters due to brine rejection. The decrease in temperature and the increase in salinity both increase the water densities. Surface waters that are denser than the underlying water masses sink. This deepwater formation process is an important part of a global deepwater circulation system that is often referred to as the "global conveyor belt" (Broecker, 1991).

The conveyor belt circulation may collapse in response to anthropogenic climate forcings (cf. Stommel, 1961; Challenor et al., 2006; Meehl et al., 2007; Vizcaino et al., 2008). Anthropogenic greenhouse gas emissions are projected to increase surface temperatures and freshwater input from precipitation in the North Atlantic (Meehl et al., 2007, Sec. 10.3.4). Both of these factors drive a decrease of the surface water densities. A decrease in the surface water density acts to decrease the density gradient between surface and deepwaters and hence acts to decrease the AMOC intensity.

The AMOC may exhibit a threshold response to anthropogenic forcing due to positive feedbacks (cf. Stommel, 1961). One key positive oceanic feedback destabilizing the AMOC is driven by the net freshwater input in the North

⋆ Corresponding author.
e-mail: nurban@psu.edu

Atlantic region (Baumgartner and Reichel, 1975; Stommel, 1961). Consider, for example, an AMOC weakening due to the anthropogenic climate forcing as discussed above. This AMOC weakening results in a slowdown of the surface currents transporting waters to the deepwater formation sites, which increases the transit time of these surface waters through the region of net freshwater inputs from the atmosphere, and decreases the rate at which salt is transported poleward. The increased transit time and reduced salt transport decrease the salinity of the surface waters. The decrease in salinity decreases the water density, which further weakens the overturning through a positive feedback loop.

Oceanic observations show mixed evidence for an AMOC slowdown over the last few decades. For example, repeated transects at 26 °N (Bryden et al., 2005) have been interpreted as a 30 percent AMOC slowdown over the last four decades. In addition, salinities in the northern North Atlantic Ocean have decreased considerably since the mid-1960s (Curry and Mauritzen, 2005). The evidence for a potential AMOC weakening is, however, not straightforward to interpret. For example, recent measurements at high temporal resolution suggest that the AMOC decrease reported by Bryden et al. (2005) may be the result of unforced internal variability, as opposed to being a response to anthropogenic forcing (Cunningham et al., 2007).

Current projections of the AMOC are deeply uncertain (Keller et al., 2007b; Zickfeld et al., 2007; Meehl et al., 2007). There is disagreement in the literature regarding the probability of such an outcome. The Intergovernmental Panel on Climate Change (IPCC) has recently stated that "it is very unlikely that the MOC will undergo a large abrupt transition during the 21st century", implying a probability of less than ten percent (Alley et al., 2007).

Previous studies deriving probabilistic AMOC projections have broken important new ground, but are still silent on key questions. The first, and arguably simplest, class of AMOC projections uses very simplified models (e.g., box or 2.5-dimensional models) with rather limited use of observational constraints (Knutti et al., 2003; Yohe et al., 2006). The use of low-dimensional AMOC models enables the extensive sampling of the large parameter space and to explore the tails of the associated probability density function (pdf). The disadvantage of using these simple models is that the resulting scenarios hinge critically on the assumption that the neglected feedbacks, for example through changes in the respiration of the soil carbon pool (Friedlingstein et al., 2006), are unimportant.

The second class of AMOC projections is based on Earth System Models of Intermediate Complexity (EMICs) with considerably improved representation of relevant processes and feedbacks (e.g., Challenor et al., 2006). However, studies using EMICs sample the tails of the parameter probability density function rather sparsely (Challenor et al., 2006).

The third class of AMOC projections is based on high resolution coupled Atmosphere Ocean General Circulation Models (AOGCM) (e.g., Schneider et al., 2007b; Meehl et al., 2007). This approach has the advantage of being based on more realistic models, but the large computational costs of AOGCMs precludes at this time to exhaustively sample the tails of the parameter distributions. The recent IPCC report (Meehl et al., 2007) concludes, for example, that no analyzed AOGCM with a reasonable AMOC hindcast shows an abrupt AMOC collapse in the 21st century for the considered forcing scenario and parameter values. Note, however, that more recent analyses may suggest that in a coupled AOGCM a high CO_2 forcing scenario can result in an AMOC collapse over a multi-century time-scale (Vizcaino et al., 2008). In addition, as shown in previous studies using simpler models, an AMOC collapse can be a low probability event and hence occur in the tails of the parameter pdf (cf. Challenor et al., 2006; Zickfeld et al., 2007) which may not be sampled by the best-guess parameter values used for the AOGCM runs analyzed in Meehl et al. (2007). Finally, current AOGCMs may overestimate the stability of the AMOC due to structural errors (Hofmann and Rahmstorf, 2009).

In summary, robust probabilistic AMOC hindcasts and projections require at least two key properties: (i) they have to be based on mechanistically sound models that include the key feedbacks, and (ii) they need to represent the full parametric uncertainty (including the tails of the joint probability density function) given relevant observational constraints.

Ideally, one would fuse all of the available and relevant constraints into all available high resolution AOGCMs in a Bayesian model averaging sense (Draper, 1995; Hoeting et al., 1999). However, this is currently not possible due to prohibitive computational requirements. Here we take a less ambitious approach and fuse a subset of relevant observations with a simple model of the coupled carbon, climate, and AMOC system. The results from this proof-of-concept study are hence subject to several caveats (discussed below) and are not fully robust. The main limitations stem from the model simplifications and the limited, highly aggregated nature of the data used. The main advances of our study compared to previous research are the expansion of the considered observational constraints, the expanded sampling of the tails of the parameter pdf, and the correction for the effects of autocorrelated residuals.

2 Model

The past and future AMOC strength depends on an intricate interplay of radiative climate forcings (e.g., due to solar variability, volcanic and industrial aerosols, or greenhouse gases such as carbon dioxide), the influence of changing surface air temperatures and precipitation patterns on surface fluxes of heat and freshwater, and the resulting AMOC changes. Deriving probabilistic AMOC hindcasts and projections therefore requires to couple models of (i) the carbon cycle, (ii) surface temperature and precipitation patterns, and (iii) the AMOC response. These model components and their coupling are described below.

2.1 Climate module

We use the DOECLIM physical climate component of the ACC2 model, which is an energy balance model of the atmosphere coupled to a one-dimensional diffusive ocean model to calculate global temperature and ocean heat content. The model is described in great detail in Kriegler (2005) and Tanaka et al. (2007), hence we outline here only

the key elements and parameters that are relevant for this study.

In this model, the land and sea surface temperatures T_{LS} and T_{SS} are determined by energy balance conditions,

$$\dot{T}_{LS} = (a_{\Gamma,L}\, C_A + C_L)^{-1} \times \left[Q_L - \lambda_L\, T_{LS} - \frac{k}{f_L}\left(T_{LS} - b_{SI}\frac{a_{\Gamma,S}}{a_{\Gamma,L}} T_{SS} \right) \right], \quad (1)$$

$$\dot{T}_{SS} = (a_{\Gamma,S}\, b_{SI}\, C_A + c_V\, z_S)^{-1} \times \left[Q_S - \lambda_S - \frac{k}{1-f_L}\left(b_{SI}\frac{a_{\Gamma,S}}{a_{\Gamma,L}} T_{SS} - T_{LS} \right) - F_O \right]. \quad (2)$$

Here the overdot denotes the time derivative, C and c are land/air and water heat capacities, Q are radiative forcings (at the top of the atmosphere), λ are climate feedback parameters, a_Γ are surface-troposphere couplings, b_{SI} is a marine surface air warming enhancement factor, k is a land-sea heat exchange coefficient, F_O is the heat flux into the interior ocean, z_S is the depth of the ocean mixed layer, and f_L is the land fraction of the Earth's surface area. The global surface air temperature is a weighted average of the land and sea surface temperatures T_{LS} and T_{SS},

$$T = f_L\, T_{LS} + (1-f_L) b_{SI}\, T_{SS}\,. \quad (3)$$

The equilibrium climate sensitivity to a doubling of atmospheric CO_2 concentration is given by a similar weighted average of land and sea sensitivities,

$$S = f_L\, S_L + (1-f_L) b_{SI}\, S_S\,, \quad (4)$$

which in turn are functions of the feedback parameters λ_L and λ_S,

$$S_L = Q_{2\times}\frac{k\, b_{SI} + (1-f_L) f_L\, \lambda_S}{k\, b_{SI}\, f_L\, \lambda_L + (1-f_L)(k + f_L\, \lambda_L)\lambda_S}\,, \quad (5)$$

$$S_S = Q_{2\times}\frac{k + (1-f_L) f_L\, \lambda_L}{k\, b_{SI}\, f_L\, \lambda_L + (1-f_L)(k + f_L\, \lambda_L)\lambda_S}\,, \quad (6)$$

where $Q_{2\times} = 3.7$ W/m^2 is the radiative forcing for a doubling of atmospheric CO_2, giving

$$S = Q_{2\times}\frac{k\, b_{SI} + (1-f_L)^2 f_L\, b_{SI}\, \lambda_L + (1-f_L) f_L^2\, \lambda_S}{k\, b_{SI}\, f_L\, \lambda_L + (1-f_L)(k + f_L\, \lambda_L)\lambda_S}\,. \quad (7)$$

The uptake of heat into the interior ocean is governed by a one-dimensional diffusion equation,

$$\dot{T}_O(z,t) = \kappa_V \frac{\partial^2}{\partial z^2} T_O(z,t)\,, \quad (8)$$

subject to the boundary conditions that $T_O = T_{SS}$ at the surface ($z = 0$) and the heat flux into the ocean floor ($z = z_B$) vanishes, where T_O is the ocean temperature as a function of depth and time and κ_V is the vertical diffusivity of heat. This diffusion equation has an exact solution which is approximated in DOECLIM by a series expansion.

The CO_2 radiative forcing of the climate is given by the logarithmic response to increases in atmospheric CO_2 as predicted by the carbon module. The other radiative forcings (e.g., non-CO_2 greenhouse gases, solar irradiance, volcanism, and tropospheric aerosols) are taken from Kriegler (2005) with some adaptations described later. Following previous work (Hegerl et al., 2006) we account for the considerable uncertainty in the magnitude of the aerosol forcing feedback due to aerosol-cloud interactions, or aerosol indirect effect (Lohmann and Feichter, 2005), by applying a multiplicative scale factor α to the radiative forcing. This scale factor is estimated in the assimilation step by fitting the forced model to the observed climate response.

2.2 Carbon cycle model

We couple a carbon cycle model to the climate module. Temperature changes in the climate module affect terrestrial and ocean carbon sources and sinks. In turn, these sources and sinks alter the atmospheric carbon dioxide concentration which forces the climate module. To model the carbon cycle we use a nonlinear impulse response approximation to the Hamburg AOGCM (Hooss et al., 2001), as modified by Ricciuto et al. (2008). The model structure and the calibration using oceanic, atmospheric, and ice core observations are detailed in Ricciuto et al. (2008). We hence give here just a brief overview.

The carbon cycle module considers the terrestrial as well as oceanic carbon cycles. There are four terrestrial carbon pools: leafy vegetation, living wood, detritus, and humus (soil carbon). The ocean model of carbon uptake has four layers: a mixed atmosphere/surface layer and three deeper layers. The three key parameters we alter in the carbon cycle model are the carbon fertilization parameter β, the respiration sensitivity Q_{10}, and the thermocline transfer rate η. The carbon fertilization parameter affects the magnitude of the atmospheric CO_2 flux taken up by living plants (net primary productivity) due to the influence of CO_2 concentrations on plant growth. The respiration sensitivity affects the increase in atmospheric CO_2 due to temperature accelerated organic decay. The thermocline transfer rate governs the rate at which dissolved carbon diffuses from the surface into the deep ocean.

An inconsistency in the coupled model structure is that the ocean heat diffusion parameter in the climate module (κ_V) is independent of the ocean carbon diffusion parameter in the carbon module (η). In the physical ocean, the heat uptake rate and carbon uptake rate are related to each other, as they both depend on the strength of vertical mixing in the ocean. A decoupled treatment of the two diffusion constants could potentially lead to artificially high model skill during model tuning, since it is possible for the ocean heat and ocean carbon observations to be fit with heat and carbon uptake rates which are incompatible with each other in the real Earth system. This limitation could be addressed in a more sophisticated model, such as an EMIC, which has a more physical representation of ocean mixing processes.

As described for example in Siegenthaler and Joos (1992), low resolution ocean models have difficulties in reproducing different tracer distributions with a common parameterization of oceanic mixing. A key reason for this is that the numerical diffusivity in these low resolution models represents a complex mixture of processes that have different temporal and spatial patterns for different tracers. Note that this tension between different tracers with respect to diffusivity estimates still can be seen in EMICs (cf. Schmittner et al., 2009). This numerical artifact imposes considerable caveats, described later.

2.3 AMOC box model

We approximate the AMOC by a simple box model developed by Zickfeld et al. (2004), forced with temperature change from the climate module. The Atlantic Ocean is represented by four well-mixed boxes: the southern, tropical, and northern surface waters, and the deep water. The boxes are connected sequentially so that surface currents flow from south to north by way of the tropics, overturn, and return to the south as deep water. This self contained cycle ignores the transport of water outside of the Atlantic.

The AMOC model does not feed back to the DOECLIM climate model, so that regional sea surface temperature changes arising from AMOC changes have no effect on global surface temperatures. Global temperatures in turn influence further AMOC changes solely through external forcing and not through any internal atmosphere-ocean dynamics. These likely important higher order interactions are perhaps best addressed in fully coupled atmosphere-ocean circulation models (e.g., Krebs and Timmermann, 2007).

The AMOC model also does not feed back to the NICCS carbon cycle model, and so does not allow AMOC changes to affect ocean carbon uptake. A mechanistically sound representation of the AMOC-carbon cycle feedback would require the development of a coupled AMOC-carbon cycle model and is not considered in this analysis. Studies suggest that this feedback can have measurable effects on atmospheric CO_2 (e.g., Sarmiento and Le Quéré, 1996; Obata, 2007; Zickfeld et al., 2008), but arguably the effect is small compared to the overall CO_2 forcing. For example, Obata (2007) found that, in a AOGCM hosing experiment in which the AMOC collapsed by 2150, the collapse alters atmospheric CO_2 in 2300 by less than 50 ppm (compared to a base concentration of 2000 ppm in 2300). In an EMIC experiment, Zickfeld et al. (2008) found that an AMOC weakening alters atmospheric CO_2 in 2500 by only 13–34 ppm, in scenarios which achieved maximum concentrations of 1500 ppm.

The dynamics of the box temperatures T_i and salinities S_i are governed by a simple system of coupled first order ordinary differential equations:

$$\dot{T}_S = \frac{m}{V_S}(T_D - T_S) + \lambda_S(T_S^* - T_S)\,, \tag{9}$$

$$\dot{T}_N = \frac{m}{V_N}(T_T - T_N) + \lambda_N(T_N^* - T_N)\,, \tag{10}$$

$$\dot{T}_T = \frac{m}{V_T}(T_S - T_T) + \lambda_T(T_T^* - T_T)\,, \tag{11}$$

$$\dot{T}_D = \frac{m}{V_D}(T_N - T_D)\,, \tag{12}$$

$$\dot{S}_S = \frac{m}{V_S}(S_D - S_S) + \frac{S_0 F_{ST}}{V_S}\,, \tag{13}$$

$$\dot{S}_N = \frac{m}{V_N}(S_T - S_N) - \frac{S_0(F_N + F_{TN})}{V_N}\,, \tag{14}$$

$$\dot{S}_T = \frac{m}{V_T}(S_S - S_T) - \frac{S_0(F_{ST} - F_{TN} - F_T)}{V_T}\,, \tag{15}$$

$$\dot{S}_D = \frac{m}{V_D}(S_N - S_D)\,, \tag{16}$$

where T_i^* are the temperatures to which the boxes relax, λ_i are thermal coupling constants, V_i are box volumes, and F_i are external freshwater fluxes into surface boxes. F_N represents the meltwater flux into the North Atlantic, and F_T represents the flux out of the tropical Pacific into the North Atlantic (Latif et al., 2000). F_{ij} are freshwater fluxes between surface boxes, and S_0 is a reference salinity. The key observable parameter in this analysis is the meridional volume transport rate (overturning) between the southern and northern boxes, referred to henceforth as the AMOC strength, given by

$$m = k[\beta(S_N - S_S) - \alpha(T_N - T_S)]\,, \tag{17}$$

where k is a hydraulic constant and α and β are thermal and haline expansion coefficients. If the model produces an AMOC reversal, m is set to zero, representing an AMOC collapse.

The relaxation temperatures and freshwater fluxes of the surface boxes are time dependent functions of the global temperature forcing ΔT, which is calculated by the climate module:

$$T_S^* = T_{S_0}^* + p_S \Delta T\,, \tag{18}$$

$$T_N^* = T_{N_0}^* + p_N \Delta T\,, \tag{19}$$

$$T_T^* = T_{T_0}^* + p_T \Delta T\,, \tag{20}$$

and

$$F_N = h_N\, p_{NH}\, \Delta T\,, \tag{21}$$

$$F_T = -h_T\, p_T\, \Delta T\,, \tag{22}$$

$$F_{ST} = F_{ST_0} + h_{ST}\, p_{SH}\, \Delta T\,, \tag{23}$$

$$F_{TN} = F_{TN_0} + h_{TN}\, p_{NH}\, \Delta T\,, \tag{24}$$

where the $T_{i_0}^*$ are unforced relaxation temperatures, the p_i are linear pattern scaling coefficients to estimate regional Atlantic and hemispheric temperatures from global temperatures, and the h_i parameterize the hydrological sensitivities to warming.

One key uncertain parameter affecting the AMOC response to anthropogenic climate forcing is the North Atlantic hydrological sensitivity, $h \equiv h_N$, which gives the change in freshwater flux into the northern box for a given change in surface air temperature. A high sensitivity implies a greater AMOC sensitivity to anthropogenic forcing (Zickfeld et al., 2004).

3 Data

3.1 Forcings

The forcings in the hindcast calibration period span the years 1850–2009. We consider CO_2 emissions (1850–2006) from (i) fossil fuel burning, cement manufacture, and gas flaring (taken from Boden et al., 2009), and (iii) land-use changes (1850–2000) from Jain and Yang (2005), based on the land-use estimate of Ramankutty and Foley (1999). The anthropogenic emissions are extended to 2009 by linear extrapolation of the 1997–2006 trend. The land use emissions 2001–2009 are held constant at 2000 values.

Because the DOECLIM forcings have not been updated past the year 2000, we extend them to 2009 using a combination of updated datasets and historical extrapolation. Solar forcing is updated through 2009 using the PMOD composite total solar irradiance dataset (Frölich and Lean, 1998). Sulfate aerosol forcing is updated to 2005 using version 2.7 of the Pacific Northwest Laboratory annual inventory of historical SO_2 emissions (S. Smith *et al.*, 2009, in preparation,

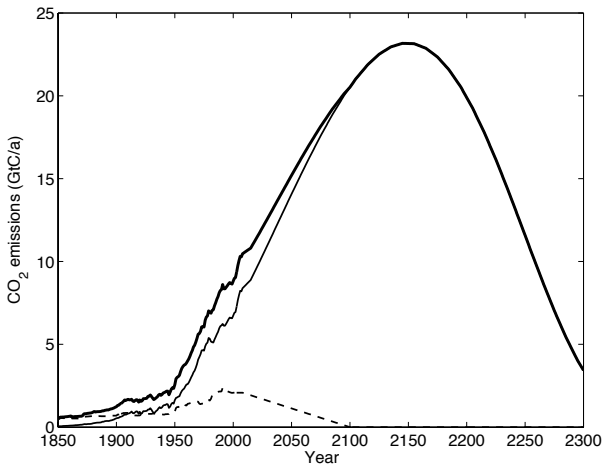

Figure 1. Annual CO_2 emissions (historical and projected business-as-usual). Depicted are total emissions (thick solid curve), fossil fuel emissions (thin solid curve), and land use emissions (thin dashed curve).

personal communication) and converted to radiative forcing by the procedure described in Kriegler, 2005; 2006–2009 SO_2 emissions are held constant at 2005 values. Volcanic forcing is assumed zero after 2000. Non-CO_2 greenhouse gases are extended to 2009 by linear extrapolation of the 1991–2000 trend.

For projections beyond the year 2009, future forcings from fossil CO_2 emissions, from non-CO_2 greenhouse gas, and anthropogenic aerosols are adopted from Nordhaus (2007) following a business-as-usual (BAU) emissions scenario, yielding cumulative fossil fuel emissions of about 4800 GtC from 2000–2300. The CO_2 emissions are plotted in Figure 1. Land-use CO_2 emissions decay linearly from 2009 levels to zero in 2100 and are zero thereafter. Volcanic forcings are assumed zero and solar forcings are held constant at the average for solar cycle 22 (1986–1996). The AMOC model is forced with the hindcast and projected temperatures.

3.2 Observational constraints

We use six different observational data sets to calibrate the model: (i) atmospheric CO_2 concentrations from Mauna Loa (Keeling and Whorf, 2005), (ii) CO_2 concentrations from the Law Dome ice core (Etheridge et al., 1996), (iii) estimates of the anthropogenic carbon fluxes into the oceans based on chlorofluorocarbon measurements (McNeil et al., 2003), (iv) a synthesis data set of combined land and marine global temperatures (Brohan et al., 2006), (v) estimates of oceanic heat uptake (Gouretski and Koltermann, 2007), and (vi) AMOC strength estimates by Bryden et al. (2005) and Cunningham et al. (2007), with error estimates derived from Kanzow et al. (2007) and Lumpkin and Speer (2007).

4 Inversion method

We use a Bayesian inversion technique based on a Markov chain Monte Carlo (MCMC) algorithm (Metropolis et al., 1953; Hastings, 1970) to estimate model parameters from the observational data over a hindcast calibration period of 1850–2009.

If the observational data are denoted y and the unknown parameters Θ, the Bayesian posterior probability of the model parameters, conditional on the observed data, is given by Bayes's theorem:

$$p(\Theta|y) \propto p(y|\Theta) \times p(\Theta)\,. \tag{25}$$

Here $p(y|\Theta)$ is the likelihood of the data given the parameters, and $p(\Theta)$ is the prior probability distribution of the parameters. After specifying the likelihood function and priors, a Markov chain of random samples are drawn from the joint posterior (Eq. 25) by MCMC. The marginal probability distribution for each parameter is a kernel density estimate constructed from the parameter's Markov chain.

Let $y = \{y_i\}$ $(i = 1 \ldots N)$ be one of the individual observation time series (e.g., temperature), and $\mu = \{f(t_i;\theta)\}$ be the model output for that data type, where the function $f(\cdot)$ is the model, t is time, and θ are the unknown model parameters. Each observational time series is assumed to be drawn from a stationary normal AR(1) first-order autoregressive process, centered on the model output, $y \sim AR1(\mu, \sigma^2, \rho)$, where σ^2 is the AR(1) innovation variance and ρ is the lag-1 (annual) autoregression coefficient. Defining the data-model residuals as $r_i = y_i - f(t_i;\theta)$, the autocorrelation can be removed to produce "whitened" residuals which are iid normal (white noise), $w_i = r_i - \rho r_{i-1}$ $(i > 1)$. Defining the stationary process variance as $\sigma_p^2 = \sigma^2/(1-\rho^2)$, the full AR(1) likelihood function can be expressed in terms of the whitened residuals as given in Bence (1995) (in slightly different notation):

$$\begin{aligned} p(y|\theta,\sigma,\rho) = {} & (2\pi\sigma_p^2)^{-1/2} \exp\left(-\frac{1}{2\sigma_p^2} r_1^2\right) \\ & \times (2\pi\sigma^2)^{-(N-1)/2} \exp\left(-\frac{1}{2\sigma^2}\sum_{i=2}^{N} w_i^2\right). \end{aligned} \tag{26}$$

Here the uncertain parameters $\Theta = \{\theta, \sigma, \rho\}$ include both the unknown model parameters θ and the unknown statistical parameters σ and ρ.

The residual errors in each of the time series are assumed to be independent of the residuals in the other time series, so the overall likelihood of all the data is the product of independent likelihood factors for each data set, each of the form given in Eq. 26. This is a simplifying assumption, but exploratory analysis does not indicate strong correlation between the residuals of different observational time series.

By using an AR(1) likelihood, the assimilation method accounts for potential autocorrelation in the residuals as well as the uncertainty in the autocorrelated process parameters. This autoregressive process is intended to encompass the combined model structural error, natural variability, and measurement error and is estimated statistically from the data-model residuals. Specifically, the CO_2 time series from Mauna Loa and the Law Dome as well as the global mean surface temperature anomalies and the oceanic heat uptake are taken to be of unknown variance and autocorrelation. For the AMOC time series, we adopt the published variance estimates (Bryden et al., 2005; Kanzow et al., 2007; Lumpkin and Speer, 2007) and neglect potential autocorrelation (fixing $\rho = 0$ and σ constant for that time series). Due to their sparsity, the ocean carbon flux data points are also assumed

Table 1. Estimated model and data distributional parameters, and their prior ranges.

parameter	symbol	units	min.	max.
respiration sensitivity	Q_{10}	—	0.2	5
carbon fertilization factor	β	—	0	1
thermocline transfer rate	η	m yr^{-1}	0.5	200
vertical diffusivity	κ_V	cm^2 s^{-1}	0.1	4
climate sensitivity	S	K	0.1	10
aerosol scaling	α	—	0	2
hydrological sensitivity	h	Sv K^{-1}	0	0.06
init. temperature	T_0	K	-0.3	0.3
init. ocean heat	H_0	10^{22} J	-50	0
init. CO_2	CO_{20}	ppm	275	295
init. AMOC strength	m_0	Sv	5	35
autocorr. (T)	ρ_T	—	0	0.99
autocorr. (CO_2, inst.)	$\rho_{CO_2,\text{inst}}$	—	0	0.99
autocorr. (ocean heat)	ρ_H	—	0	0.99
std. dev. (T)	σ_T	K	0.05	0.5
std. dev. (CO_2, ice)	$\sigma_{CO_2,\text{ice}}$	ppm	0.2	20
std. dev. (CO_2, inst.)	$\sigma_{CO_2,\text{inst}}$	ppm	0.2	7
std. dev. (ocean heat)	σ_H	10^{22} J	0.1	10

to be independent (and identically distributed) with normal observational errors adopted from McNeil et al. (2003).

The estimated parameters are model parameters, AR(1) statistical parameters, and the initial values in the temperature, ocean heat, CO_2, and AMOC time series. The parameters with their prior ranges are detailed in Table 1. We assume *a priori* that all the parameters are independent of each other so the joint prior $p(\Theta)$ for all the parameters factorizes into a product of independent priors for each parameter. This prior assumption does not preclude the possibility of posterior correlations between parameters after they have been estimated (see Section 5.2). All parameter priors are truncated uniform distributions except for climate sensitivity, which is given a diffuse truncated Cauchy(3,2) prior intended to approximate the information contained in paleo constraints that are neglected in our analysis (e.g., Annan et al., 2005; Schneider von Deimling et al., 2006; Annan and Hargreaves, 2009).

The calibrated parameters found in the inversion are used to probabilistically project future climate observables. The hindcasts and projections are samples from the posterior predictive distribution, with the observational/process noise superimposed. The temperature, ocean heat, and CO_2 errors and autocorrelations are estimated as above, with the CO_2 error assumed the same as the instrumental time series. The AMOC error is assumed to be ± 6 Sv (1σ) in hindcasts (1850–2009) following Bryden et al. (2005), and 2 Sv in projections (after 2009) following Cunningham et al. (2007).

5 Results and discussion

5.1 Hindcasts

The hindcasts of mean surface temperatures, oceanic heat anomalies, atmospheric CO_2 concentrations, and AMOC strength show considerable skill. For example, the observed surface temperature cooling after the Agung and Pinatubo volcanic eruptions (in 1963 and 1991, respectively) are reasonably well reproduced in the hindcasts (Figure 2). There is a slight suggestion that a similar pattern is seen in the oceanic heat anomaly, but this signal is relatively small compared to the data uncertainties and the magnitude of the data-model residuals.

The anthropogenic trend in atmospheric CO_2 concentrations is large compared to the observation uncertainties, resulting in a high signal-to-noise ratio. The relatively large signal-to-noise ratio in the CO_2 hindcasts allows relatively well-constrained carbon cycle parameter estimates (discussed below) and thereby relatively tightly constrained CO_2 projections. The signal-to-noise ratio decreases roughly from the CO_2 observations to the observations of surface temperature, oceanic heat anomaly, and the AMOC intensity.

Although the two decadal ocean carbon flux data points are not highly informative, they are also hindcast well by the calibrated model at its posterior mode. No strong volcanic response is seen in the best fit ocean carbon uptake, but volcanic responses are visible in the upper 95% credible interval, presumably in the parametric tails that give a stronger carbon cycle response to temperature changes.

The calibrated model hindcasts little forced change in AMOC strength, consistent with the interpretation of Cunningham et al. (2007) that the declines in AMOC strength observed by Bryden et al. (2005) may be ascribed to natural variability and observation error.

5.2 Parameter estimates

Parameter estimates associated with the high signal-to-noise ratio are considerably sharpened compared to their prior estimates (Figure 3). This is the case, for example, for the CO_2 fertilization factor and the climate sensitivity. In contrast, the estimate for the hydrological sensitivity is much less constrained by the observations. The considered AMOC observations have very little power to sharpen the prior estimate of the hydrological sensitivity, consistent with the findings of Keller and McInerney (2008). Our AMOC projections are therefore sensitive to prior assumptions about this parameter and deeply uncertain (Keller et al., 2007b; Lempert, 2002). Both the low and high ends of the prior range of hydrological sensitivity (0 and 0.06 Sv/K) are close to the the predictions of different coupled models (Zickfeld et al., 2004), so this full range of prior uncertainty should be propagated through to the model projections even if data cannot constrain it further.

The estimated climate sensitivity is on the low end of recent estimates (Meehl et al., 2007, Table 8.2, Figure 9.20). This is in part a consequence of the low value of the aerosol forcing scaling factor $\alpha \approx 0.6$ required for the total forcing to reproduce the observed temperature and ocean heat time series (Fig. 3). The observed warming can be explained by a low climate sensitivity and a small aerosol cooling effect. In contrast, higher climate sensitivities are compatible with a strong aerosol cooling effect counteracting some of the warming (cf. Forest et al., 2002). A low climate sensitivity in turn implies less projected warming and AMOC weakening.

Some of the parameter estimates show strong correlations (Figure 4). For example, estimates of the ocean thermocline exchange rate for CO_2 and the CO_2 fertilization factor are negatively correlated (Figure 4, row 2, column 2). This finding is similar to the findings of Ricciuto et al. (2008)

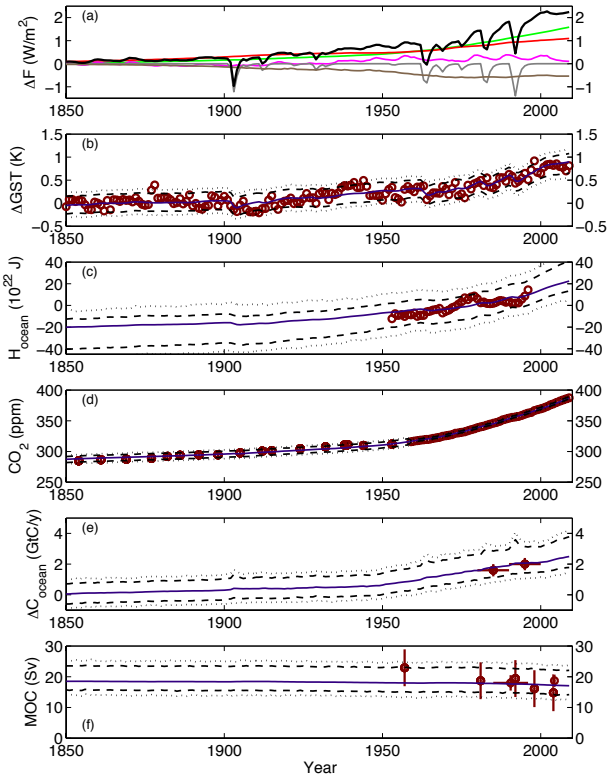

Figure 2. *Panel (a):* Historic radiative forcings. The thick black line is the total radiative forcing. The thin gray lines are, from top to bottom, CO_2, non-CO_2 greenhouse gases, solar variability, volcanic aerosols, and anthropogenic aerosols. The forcing data are described more fully in Section 3.1. The modeled CO_2 and aerosol forcings are taken from the best fit hindcast. *Panels (b)-(e):* Observations and hindcasts. The observational constraints are shown by open circles (red): (b) surface temperature anomaly, (c) ocean heat anomaly, (d) atmospheric CO_2 concentration, (e) ocean carbon uptake, (f) AMOC strength. The best fit (maximum posterior probability) model outputs are shown by solid curves (purple), and the dashed and dotted curves are 90% and 98% predictive credible intervals. The vertical error bars in panel (f) represent one standard deviation of the reported observation errors (Bryden et al., 2005; Kanzow et al., 2007; Lumpkin and Speer, 2007).

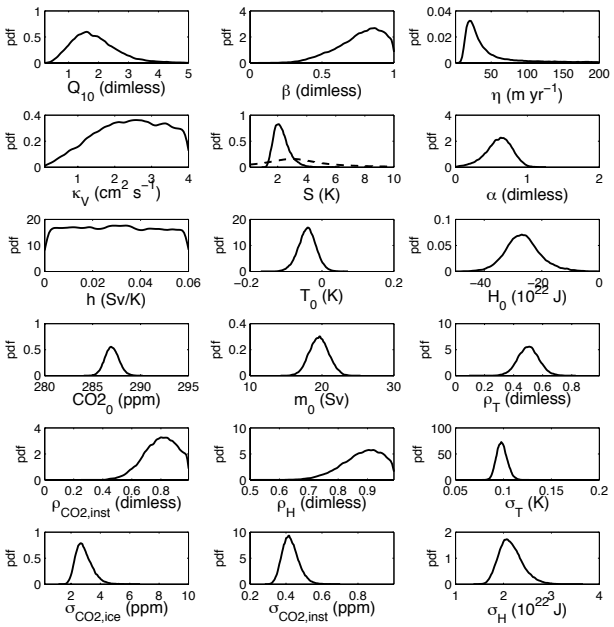

Figure 3. Marginal probability density functions of the estimated parameters. The horizontal axis range represents the lower and upper bounds of the prior probability density function. The dashed curve in the climate sensitivity plot is the non-uniform prior distribution. All other parameter priors are bounded uniform and not depicted.

and is expected because an increased thermocline exchange rate (stronger ocean carbon sink) requires a decreased CO_2 fertilization factor (weaker terrestrial carbon sink) to result in the same atmospheric CO_2 observations. A second example is the positive correlation between the climate sensitivity and the aerosol scaling factor (Figure 4, row 5, column 5). As discussed above, this positive correlation is expected because a higher climate sensitivity can be counteracted by a stronger (negative) climate forcing from aerosols.

A third example of parameter correlation is between the climate sensitivity and the vertical diffusivity of heat in the ocean (Figure 4, row 4, column 4). This correlation is expected to be positive when observing surface temperatures, and negative when observing ocean heat content (Urban and Keller, 2009). In Figure 4 this correlation may appear weak. In fact, the correlation between S and κ_V is moderately positive (about 0.4). The positive correlation implies that temperature provides a relatively stronger constraint on climate sensitivity than does ocean heat, consistent with the signal-to-noise ratios present in those observations (see Section 5.1). Further evidence to support this hypothesis is found in the marginal posterior pdf for κ_V in Figure 3, which is broad, indicating that the ocean heat data do not strongly constrain the diffusivity. This may be related to the highly autocorrelated ocean heat residuals (Fig. 3, panel ρ_H), as higher autocorrelations imply fewer effective degrees of freedom in the data.

As discussed in Section 2.2, the decoupled treatment of ocean heat and carbon diffusion in the model can lead to inconsistency between these parameters which would not exist in a model that treats both processes using the same parameterization of vertical mixing. The estimates for the heat diffusion (κ_V) and carbon diffusion (η) constants in Figure 3 may lend support to the presence of such inconsistency, as the assimilation simultaneously implies a higher rate of ocean heat uptake but a lower rate of ocean carbon uptake. However, this interpretation is sensitive to the choice of prior range for these parameters, and the relationship between the values of parameter. (For example, an upper limit of $\eta = 200$ m/yr may not imply the same amount of vertical mixing as an upper limit of $K_V = 4$ cm^2/s.) Another line of evidence comes from Figure 4, which shows the inferred κ_V and η to be uncorrelated with each other. One might expect them to be correlated if they arise from the same underlying mixing processes, assuming that the highly aggregated observations are sufficiently informative to detect this correlation. However, it is difficult to evaluate the expected amount of correlation between the two diffusion parameters in this model, considering that both are "effective" parameters which attempt to encode a variety of non-diffusive mix-

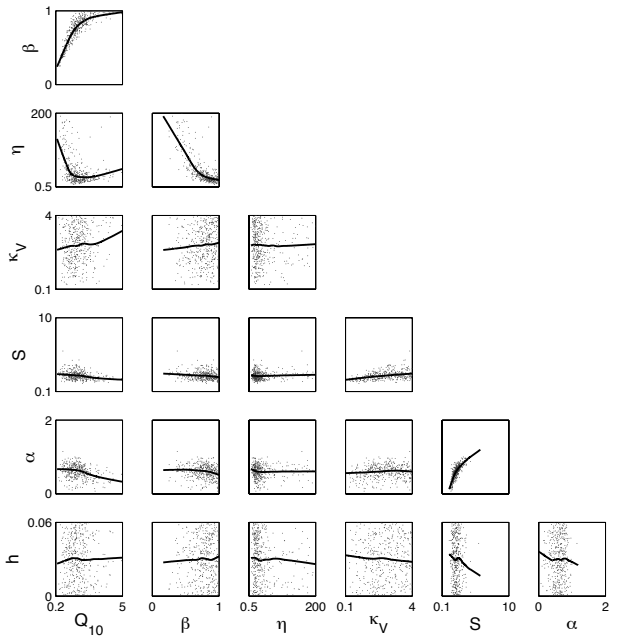

Figure 4. Two dimensional projections of the posterior probability density functions of the estimated model parameters illustrating the correlation in the posterior estimates. Lowess-smoothed curves are superimposed on the pairwise scatterplots as a guide to the eye.

ing and biogeochemical processes, and hence are difficult to interpret.

5.3 Projections

The atmospheric CO_2 concentrations and the mean surface air temperatures are projected to increase, with a considerable widening of the projection confidence bounds (Figure 5). The temperature projections are relative to 1850, and are low compared to recent IPCC projections (Meehl et al., 2007, Sec. 10.3) due to the low central estimate of climate sensitivity found in our study. We find a 1.5 K mean warming over the 21st century in our BAU emissions scenario, similar to the warming projected by the IPCC in the B2 emissions scenario. However, the forcing scenario which most closely approximates our 2100 CO_2 concentration projections (Fig. 5a) is the A1B scenario, with approximately 2.5 K of warming projected by the IPCC over the 21st century.

The AMOC intensity is projected to decrease gradually over time, with a sizeable probability of an AMOC collapse (defined here as an AMOC intensity of zero) within the considered time horizon. The AMOC strength decreases by an average of 17 percent from 2000 to 2100. This reduction is consistent with but slightly lower than the projections of the coupled climate models compared in Schneider et al. (2007b), and smaller than the results of Knutti et al. (2003), which show AMOC reductions of approximately 25 and 60 percent, respectively over the same time horizon. (The 2200 projections for AMOC strength include some negative values, not shown in the graph. This is due to the addition of observational noise, as the model itself does not produce AMOC reversals.)

An AMOC collapse has been interpreted as a low-

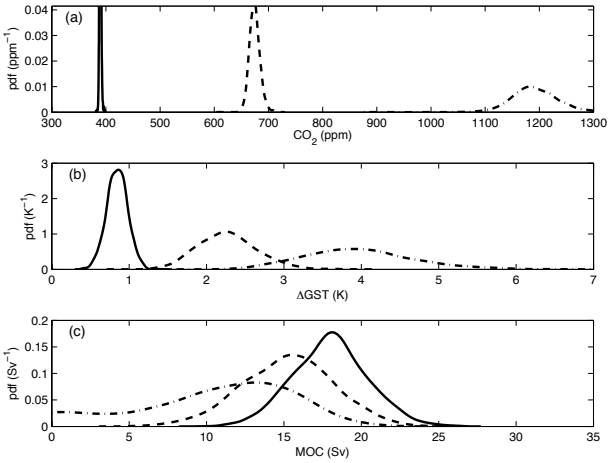

Figure 5. Probabilistic projections of (a) atmospheric CO_2 concentrations, (b) global mean surface temperature anomalies, and (c) AMOC strength in 2010 (solid), 2100 (dashed), and 2200 (dash-dotted).

probability event (Alley et al., 2007; Rahmstorf and Zickfeld, 2005; Wood et al., 2003). The model projections suggest that an AMOC collapse in the 21st century is very unlikely (i.e., a probability of less than ten percent, Figure 6, dashed curve), consistent with the recent IPCC assessment (Alley et al., 2007). (The AMOC is defined to be collapsed if the modeled AMOC strength is zero.) The projected probability of an AMOC collapse increases gradually and almost linearly after 2150 to reach 10 percent in the next two centuries, and over 35 percent by 2300.

Although the probability of experiencing an AMOC collapse in the 21st century is small according to our analysis, the probability of committing to a future collapse within the next century can be higher. To test this, we explore several alternate forcing scenarios in which the BAU emissions trajectory is followed to a given year, after which the CO_2 emissions are abruptly reduced to zero and remain zero thereafter. An AMOC collapse is "triggered" by that year if the AMOC later collapses before 2300. A future collapse is possible in a zero-emissions scenario because, although there are no further CO_2 emissions, atmospheric greenhouse gas concentrations and climatic forcing of the AMOC remain high until natural carbon sinks can remove CO_2 from the atmosphere. Our analysis indicates that if emissions are reduced to zero after 2100, there remains a 4% chance that the AMOC will collapse by 2300 (Figure 6, solid curve), or 18% if emissions are halted in 2150. If CO_2 emissions stop in 2200, the probability of committing to an AMOC collapse rises to 30%.

6 Caveats

The results of this proof-of-concept study hinge on a large number of assumptions that impose severe caveats on the forthcoming conclusions and point to potential future improvements. Relevant examples for such potential improvements include: (i) using a more refined Earth system model, (ii) considering information contained in the spatial structure of the observational constraints, (iii) representing

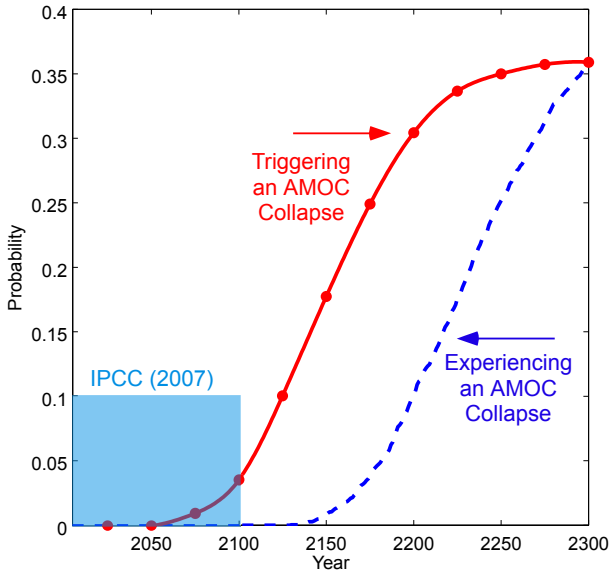

Figure 6. Model-derived risk estimate of a AMOC collapse over time. The dashed curve (blue) is the probability that the AMOC will be in a state of collapse in a given year. The solid curve (red) depicts the commitment to future AMOC collapse, i.e., the probability of crossing a collapse threshold. It is the probability that if BAU emissions are reduced to zero beyond a given year, the AMOC will nevertheless be in a state of collapse in the year 2300. The shaded blue box represents the judgement of the 2007 IPCC Fourth Assessment Report (Alley et al., 2007), $< 10\%$ probability of collapse by 2100.

the uncertainty in the CO_2 emissions scenarios, and (iv) adding paleo-proxies to the analyzed data set. These future research areas are briefly discussed below.

First, the adopted model is extremely simple, does not fully couple the climate, carbon cycle, and AMOC components, and misses likely important feedbacks such as changes in the nitrogen cycle (Houghton et al., 1998) or the Greenland ice sheet dynamics (Zwally et al., 2002). Increasing the model complexity is a logical step to reduce this problem (e.g., Challenor et al., 2006), but many of these potentially relevant feedbacks are still poorly resolved in Earth system models. Our study is also silent on the relative contributions of the climate parameter uncertainty vs. the carbon cycle parameter uncertainty to the total uncertainty in the AMOC projections. Second, our analysis considers only globally aggregate information (e.g., the global average surface temperature). This approach reduces the computational burden considerably, but it neglects potentially useful information contained in the spatial signal structure. For example, the pattern of oceanic heat and other tracer anomalies may provide useful constraints on the ocean diffusivity (Cessi et al., 2006; Schmittner et al., 2009). Third, this study considers a single CO_2 emissions scenario to isolate the effects of key uncertainties in the carbon, climate, and AMOC system from the uncertainties in the socioeconomic system. The projections are strongly contingent on the adopted business-as-usual CO_2 emissions scenario, and are hence silent on the effects of potential cuts in CO_2 emissions due to climate policies, as well as on the uncertainty in the future BAU emissions trajectory. Using probabilistic CO_2 emissions scenarios (Keller et al., 2007a; Webster et al., 2002) would likely change the estimated probabilities of a future AMOC collapse. Fourth, this study uses century-scale observations that are mostly derived from the instrumental record. Adding paleo-observations such as reconstructed temperatures over a millennium time-scale may provide important additional constraints (Crowley, 2000; Hegerl et al., 2006). Last, but not least, the projections are quite sensitive to forcing assumptions in the historical calibration period, such as reconstructions of atmospheric SO_2 concentrations and the strength of the aerosol indirect effect.

Estimates of the probability of "tail-area events" (such as an AMOC collapse in this analysis) are at this time often deeply uncertain, i.e., they can hinge on subjective assumptions about factors such as model structures and parameter priors (Keller and McInerney, 2008; Schneider et al., 2007b). Quantifying the effects of this deep uncertainty on the future projections is an area of active research (cf. Tomassini et al., 2007) and a key avenue to potentially improve climate change decision-making (cf. Ellsberg, 1961; Lempert, 2002).

7 Conclusions

We develop a simple and computationally efficient model of the coupled climate, carbon, and AMOC systems. We demonstrate the feasibility to calibrate this model using a Bayesian inversion technique to derive probabilistic hindcasts and projections that carefully sample the tail areas of the parameter probability density function. The probability of an AMOC collapse in the 21st century under a business-as-usual CO_2 emissions scenario is less than one in ten in our simple model. This estimate is consistent with the recent IPCC assessment (Alley et al., 2007). However, the projected probability of an AMOC collapse increases beyond this century and exceeds one in three over the next three centuries. Although the probability of experiencing an AMOC collapse in the 21st century is small, the probability of crossing a forcing threshold and committing to a future collapse may be as high as one in twenty during this century and over one in three during the next.

8 Acknowledgements

We thank Kirsten Zickfeld and Elmar Kriegler for providing the source codes of the DOECLIM and the AMOC box models and for many insightful discussions, Brian Tuttle for assistance with model development, and James Annan and anonymous reviewers for comments and suggestions. Funding for this project was provided by the U.S. Environmental Protection Agency under Purchase Order EP07H000339 and by the National Science Foundation. Any opinions, findings and conclusions or recommendations expressed in this material, and remaining errors, are those of the authors alone.

REFERENCES

Adger, N., Aggarwal, P., Agrawala, S., Alcamo, J., Allali, A., Anisimov, O., Arnell, N., Boko, M., Canziani, O., Carter, T., Casassa, G., Confalonieri, U., Cruz, R. V., Alcaraz, E. d. A.,

Easterling, W., Field, C., Fischlin, A., Fitzharris, B. B., Garcá, C. G., Hanson, C., Harasawa, H., Hennessy, K., Huq, S., Jones, R., Bogataj, L. K., Karoly, D., Klein, R., Kundzewicz, Z., Lal, M., Lasco, R., Love, G., Lu, X., Magrín, G., J.Mata, L., McLean, R., Menne, B., Midgley, G., Mimura, N., Mirza, M. Q., Moreno, J., Mortsch, L., Niang-Diop, I., Nicholls, R., Nováky, B., Nurse, L., Nyong, A., Oppenheimer, M., Palutikof, J., Parry, M., Patwardhan, A., Lankao, P. R., Rosenzweig, C., Schneider, S., Semenov, S., Smith, J., Stone, J., Ypersele, J.-P. v., Vaughan, D., Vogel, C., Wilbanks, T., Wong, P. P., Wu, S. and Yohe, G. *Climate Change 2007: Impacts, Adaptation and Vulnerability, Summary for Policymakers*. IPCC Secretariat, c/o WMO, 7bis, Avenue de la Paix, C.P. N ° 2300, 1211 Geneva 2, SWITZERLAND.

Alley, R., Berntsen, T., Bindoff, N. L., Chen, Z., Chidthaisong, A., Friedlingstein, P., Gregory, J., Hegerl, G., Heimann, M., Hewitson, B., Hoskins, B., Joos, F., Jouzel, J., Kattsov, V., Lohmann, U., Manning, M., Matsuno, T., Molina, M., Nicholls, N., Overpeck, J., Qin, D., Raga, G., Ramaswamy, V., Ren, J., Rusticucci, M., Solomon, S., Somerville, R., Stocker, T. F., Stott, P., Stouffer, R. J., Whetton, P., Wood, R. A. and Wratt, D. *Climate Change 2007: The Physical Science Basis, Summary for Policymakers*. IPCC Secretariat, c/o WMO, 7bis, Avenue de la Paix, C.P. N ° 2300, 1211 Geneva 2, SWITZERLAND.

Annan, J. D. and Hargreaves, J. C. 2009. On the generation and interpretation of probabilistic estimates of climate sensitivity. *Climatic Change*. doi:10.1007/s10584-009-9715-y.

Annan, J. D., Hargreaves, J. C., Ohgaito, R., Abe-Ouchi, A. and Emori, S. 2005. Efficiently constraining climate sensitivity with paleoclimate simulations. *Scientific Online Letters on the Atmosphere* **1**, 181–184.

Baumgartner, A. and Reichel, E. 1975. *The world water balance*. Elsevier, Amsterdam, the Netherlands, and New York.

Bence, J. R. 1995. Analysis of short time series: correcting for autocorrelation. *Ecology* **76**, 628–639.

Boden, T. A., Marland, G. and Andres, R. J.: 2009, Carbon Dioxide Information Analysis Center, Oak Ridge National Laboratory, U.S. Department of Energy, Oak Ridge, TN, U.S.A. doi: 10.3334/CDIAC/00001. Available electronically from: http://cdiac.ornl.gov/trends/emis/overview_2006.html.

Broecker, W. S. 1991. The great ocean conveyor. *Oceanography* **4**, 79–89.

Brohan, P., Kennedy, J. J., Harris, I., Tett, S. F. B. and Jones, P. D. 2006. Uncertainty estimates in regional and global observed temperature changes: A new data set from 1850. *Journal of Geophysical Research-Atmospheres* **111**, D12106.

Bryden, H. L., Longworth, H. R. and Cunningham, S. A. 2005. Slowing of the Atlantic meridional overturning circulation at 25° N. *Nature Nature* **438**(7068), 655–657.

Cessi, P., Young, W. R. and Polton, J. A. 2006. Control of large-scale heat transport by small-scale mixing. *Journal of Physical Oceanography* **36**(10), 1877–1894.

Challenor, P. G., Hankin, R. K. S. and March, R.: 2006, Towards the probability of rapid climage change, *in* H. J. Schellnhuber, W. Cramer, N. Nakicenovic, T. Wigley and G. Yohe (eds), *Avoiding dangerous climate change*, Cambridge University Press, pp. 55–63.

Crowley, T. J. 2000. Causes of climate change over the past 1000 years. *Science* **289**(5477), 270–277.

Cunningham, S. A., Kanzow, T., Rayner, D., Baringer, M. O., Johns, W. E., Marotzke, J., Longworth, H. R., Grant, E. M., Hirschi, J. J. M., Beal, L. M., Meinen, C. S. and Bryden, H. L. 2007. Temporal variability of the Atlantic meridional overturning circulation at 26.5°N. *Science* **317**(5840), 935–938.

Curry, R. and Mauritzen, C. 2005. Dilution of the northern North Atlantic Ocean in recent decades. *Science* **308**(5729), 1772–1774.

Draper, D. 1995. Assessment and propagation of model uncertainty. *Journal of the Royal Statistical Society Series B-Methodological* **57**(1), 45–97.

Ellsberg, D. 1961. Risk, ambiguity, and the Savage axioms. *Quarterly Journal of Economics* **75**, 643–669.

Etheridge, D. M., Steele, L. P., Langenfelds, R. L., Francey, R. J., Barnola, J. M. and Morgan, V. I. 1996. Natural and anthropogenic changes in atmospheric CO_2 over the last 1000 years from air in Antarctic ice and firn. *Journal of Geophysical Research-Atmospheres* **101**(D2), 4115–4128.

Forest, C. E., Stone, P. H., Sokolov, A. P., Allen, M. R. and Webster, M. D. 2002. Quantifying uncertainties in climate system properties with the use of recent climate observations. *Science* **295**, 113–117.

Friedlingstein, P., Cox, P., Betts, R., Bopp, L., von Bloh, W., Brovkin, V., Cadule, P., Doney, S., Eby, M., Fung, I., Bala, G., John, J., Jones, C., Joos, F., Kato, T., Kawamiya, M., Knorr, W., Lindsay, K., Matthews, H. D., Raddatz, T., Rayner, P., Reick, C., Roeckner, E., Schnitzler, K.-G., Schnur, R., Strassmann, K., Weaver, A. J., Yoshikawa, C. and Zeng, N. 2006. Climate-carbon cycle feedback analysis: Results from the C^4MIP model intercomparison. *Journal of Climate* **19**, 3337–3353.

Frölich, C. and Lean, J. 1998. The Sun's total irradiance: Cycles and trends in the past two decades and associated climate change uncertainties. *Geophysical Research Letters* **25**, 4377–4380. Updated data are available online: C. Frölich, PMOD/WRC, http://www.pmodwrc.ch/pmod.php?topic=tsi/composite/SolarConstant.

Gouretski, V. and Koltermann, K. P. 2007. How much is the ocean really warming?. *Geophysical Research Letters* **34**, L01610.

Hastings, W. K. 1970. Monte Carlo sampling methods using Markov chains and their applications. *Biometrika* **57**(1), 97–109.

Hegerl, G. C., Crowley, T. J., Hyde, W. T. and Frame, D. J. 2006. Climate sensitivity constrained by temperature reconstructions over the past seven centuries. *Nature* **440**(7087), 1029–1032.

Hoeting, J. A., Madigan, D., Raftery, A. E. and Volinsky, C. T. 1999. Bayesian model averaging: A tutorial. *Stat Sci* **14**(4), 382–401.

Hofmann, M. and Rahmstorf, S. 2009. On the stability of the Atlantic meridional overturning circulation. *Proceedings of the National Academy of Sciences of the United States of America* **106**, 20584–20589.

Hooss, G., Voss, R., Hasselmann, K., Maier-Reimer, E. and Joos, F. 2001. A nonlinear impulse response model of the coupled carbon cycle-climate system (NICCS). *Climate Dynamics* **18**(3-4), 189–202.

Houghton, R. A., Davidson, E. A. and Woodwell, G. M. 1998. Missing sinks, feedbacks, and understanding the role of terrestrial ecosystems in the global carbon balance. *Global Biogeochemical Cycles* **12**(1), 25–34.

Jain, A. K. and Yang, X. J. 2005. Modeling the effects of two different land cover change data sets on the carbon stocks of plants and soils in concert with CO_2 and climate change. *Global Biogeochemical Cycles* **19**(2), GB2015.

Kanzow, T., Cunningham, S. A., Rayner, D., Hirschi, J. J. M., Johns, W. E., Baringer, M. O., Bryden, H. L., Beal, L. M., Meinen, C. S. and Marotzke, J. 2007. Observed flow compensation associated with the MOC at 26.5°N in the Atlantic. *Science* **317**(5840), 938–941.

Keeling, C. D. and Whorf, T. P. 2005. Atmospheric CO_2 records from sites in the SIO air sampling network, *Technical report*, Carbon Dioxide Information Analysis Center, Oak Ridge National Laboratory. Updated data available online: P. Tans, NOAA/ESRL, ftp://ftp.cmdl.noaa.gov/ccg/co2/

trends/co2_annmean_mlo.txt.

Keller, K. and McInerney, D. 2008. The dynamics of learning about a climate threshold. *Climate Dynamics* **30**, 321–332.

Keller, K., Tan, K., Morel, F. M. M. and Bradford, D. F. 2000. Preserving the ocean circulation: Implications for climate policy. *Climatic Change* **47**(1-2), 17–43.

Keller, K., Bolker, B. M. and Bradford, D. F. 2004. Uncertain climate thresholds and optimal economic growth. *Journal of Environmental Economics and Management* **48**, 723–741.

Keller, K., Miltich, L. I., Robinson, A. and Tol, R. S. J. 2007a. How overconfident are current projections of carbon dioxide emissions?. *Working Paper Series, Research Unit Sustainability and Global Change, Hamburg University.* **FNU-124**, http://ideas.repec.org/s/sgc/wpaper.html.

Keller, K., Schlesinger, M. and Yohe, G. 2007b. Managing the risks of climate thresholds: Uncertainties and information needs. *Climatic Change* **91**, 5–10. doi:10.1007/s10584-006-9114-6.

Knutti, R., Stocker, T. F., Joos, F. and Plattner, G. K. 2003. Probabilistic climate change projections using neural networks. *Climate Dynamics* **21**(3-4), 257–272.

Krebs, U. and Timmermann, A. 2007. Tropical air-sea interactions accelerate the recovery of the Atlantic meridional overturning circulation after a major shutdown. *Journal of Climate* **20**, 4940–4956.

Kriegler, E.: 2005, Imprecise probability analysis for integrated assessment of climate change. Ph.D. thesis, University of Potsdam, Potsdam, Germany.

Kuhlbrodt, T., Rahmstorf, S., Zickfeld, K., Vikebø, F. B., Sundby, S., Hofmann, M., Link, P. M., Bondeau, A., Cramer, W. and Jaeger, C. 2009. An integrated assessment of changes in the thermohaline circulation. *Climatic Change* **96**, 489–537.

Latif, M., Roeckner, E., Mikolajewski, U. and Voss, R. 2000. Tropical stabilization of the thermohaline circulation in a greenhouse warming simulation. *Journal of Climate* **13**, 1809–1813.

Lempert, R. J. 2002. A new decision sciences for complex systems. *Proceedings of the National Academy of Sciences of the United States of America* **99**, 7309–7313.

Link, P. M. and Tol, R. S. J. 2004. Possible economic impacts of a shutdown of the thermohaline circulation: an application of FUND. *Portuguese Economic Journal* **3**, 99–114.

Lohmann, U. and Feichter, J. 2005. Global indirect aerosol effects: a review. *Atmospheric Chemistry and Physics* **5**, 715–737.

Lumpkin, R. and Speer, K. 2007. Global ocean meridional overturning. *Journal of Physical Oceanography* **37**(10), 2550–2562.

Manabe, S. and Stouffer, R. J. 1994. Multiple-century response of a coupled ocean-atmosphere model to an increase of atmospheric carbon dioxide. *Journal of Climate* **7**, 5–23.

McNeil, B. I., Matear, R. J., Key, R. M., Bullister, J. L. and Sarmiento, J. L. 2003. Anthropogenic CO_2 uptake by the ocean based on the global chlorofluorocarbon data set. *Science* **299**(5604), 235–239.

Meehl, G. A., Stocker, T. F., Collins, W. D., Friedlingstein, P., Gaye, A., Gregory, J., Kitoh, A., Knutti, R., Murphy, J., Noda, A., Raper, S., Watterson, I., Weaver, A. and Zhao, Z.-C.: 2007, *Climate Change 2007: The Physical Science Basis. Contribution of Working Group I to the Fourth Assessment Report of the Intergovernmental Panel on Climate Change*, Cambridge University Press, Cambridge, United Kingdom and New York, NY, USA.

Metropolis, N., Rosenbluth, A. W., Rosenbluth, M. N., Teller, A. H. and Teller, E. 1953. Equation of state calculations by fast computing machines. *J. Chem. Phys.* **21**, 1087–1092.

Nordhaus, W. D. 2007. The challenge of global warming: Economic models and environmental policy, *Technical report*, http://nordhuas.econ.yale.edu/DICE2007.htm, accessed May 2, 2007, model version: DICE-2007.delta.v7.

Obata, A.. 2007. Climate-carbon cycle model response to freshwater discharge into the North Atlantic. *Journal of Climate* **20**, 5962–5976.

Rahmstorf, S. and Zickfeld, K. 2005. Thermohaline circulation changes: A question of risk assessment - an editorial review essay. *Climatic Change* **68**(1-2), 241–247.

Ramankutty, N. and Foley, J. A. 1999. Estimating historical changes in global land cover: Croplands from 1700 to 1992. *Global Biogeochemical Cycles* **13**(4), 997–1027.

Ricciuto, D., Davis, K. and Keller, K. 2008. A Bayesian calibration of a simple carbon cycle model: The role of observations in estimating and reducing uncertainty. *Global Biogeochemical Cycles* **22**, GB2030.

Sarmiento, J. L. and Le Quéré, C. 1996. Oceanic carbon dioxide uptake in a model of century-scale global warming. *Science* **274**, 1346–1350.

Schmittner, A., Urban, N. M., Keller, K. and Matthews, D. 2009. Using tracer observations to reduce the uncertainty of ocean diapycnal mixing and climate-carbon cycle projections. *Global Biogeochemical Cycles* **23**, GB4009.

Schneider, S. H., Semenov, S., Patwardhan, A., Burton, I., Magadza, C. H. D., Oppenheimer, M., Pittock, A. B., Rahman, A., Smith, J. B., Suarez, A. and Yamin, F. 2007a. Assessing key vulnerabilities and the risk from climate change. In *Climate Change 2007: Impacts, Adaptation and Vulnerability. Contribution of Working Group II to the Fourth Assessment Report of the Intergovernmental Panel on Climate Change*, M.L. Parry, O.F. Canziani, J.P. Palutikof, P.J. van der Linden and C.E. Hanson, Eds., Cambridge University Press, Cambridge, UK 779–810.

Schneider, B., Latif, M. and Schmittner, A. 2007b. Evaluation of different methods to assess model projections of the future evolution of the Atlantic meridional overturning circulation. *Journal of Climate* **20**(10), 2121–2132.

Schneider von Deimling, T., Held, H., Ganopolski, A. and Rahmstorf, S. 2006. Climate sensitivity estimated from ensemble simulations of glacial climate. *Climate Dynamics* **27**, 149–163.

Siegenthaler, U. and Joos, F. 1992. Use of a simple model for studying oceanic tracer distributions and the global carbon cycle. *Tellus B* **44**, 186–207.

Stommel, H. 1961. Thermohaline convection with two stable regimes of flow. *Tellus* **13**(2), 224–230.

Stouffer, R. J., Yin, J., Gregory, J. M., Dixon, K. W., Spelman, M. J., Hurlin, W., Weaver, A. J., Ebyd, M., Flato, G. M., Hasumi, H., Hu, A., Jungclaus, J. H., Kamenkovich, I. V., Levermann, A., Montoya, M., Murakami, S., Nawrath, S., Oka, A., Peltier, W. R., Robitaille, D. Y., Sokolov, A., Vettoretti, G. and Weber, S. L. 2006. Investigating the causes of the response of the thermohaline circulation to past and future climate changes. *Journal of Climate* **19**(8), 1365–1387.

Tanaka, K., Kriegler, E., Bruckner, T., Hooss, G., Knorr, W. and Raddatz, T. 2007. Aggregated carbon cycle, atmospheric chemistry, and climate model (ACC2). description of the forward and inverse modes (Reports on Earth System Science No. 40), *Technical report*, Hamburg, Germany.

Tomassini, L., Reichert, P., Knutti, R., Stocker, T. F. and Borsuk, M. E. 2007. Robust Bayesian uncertainty analysis of climate system properties using Markov chain Monte Carlo methods. *Journal of Climate* **20**, 1239–1254.

Urban, N. M. and Keller, K. 2009. Complementary constraints on climate sensitivity. *Geophysical Research Letters* **36**, L04708.

Vellinga, M. and Wood, R. A. 2002. Global climatic impacts of a collapse of the Atlantic thermohaline circulation. *Climatic Change* **54**(3), 251–267.

Vizcaino, M., Mikolajewicz, U., Groger, M., Maier-Reimer, E., Schurgers, G. and Winguth, A. M. E. 2008. Long-term ice sheet-climate interactions under anthropogenic greenhouse forcing simulated with a complex Earth System Model. *Climate Dynamics* **31**, 665–690.

Webster, M. D., Babiker, M., Mayer, M., Reilly, J. M., Harnisch, J., Hyman, R., Sarofim, M. C. and Wang, C. 2002. Uncertainty in emissions projections for climate models. *Atmos. Environ.* **36**(22), 3659–3670.

Wood, R. A., Vellinga, M. and Thorpe, R. 2003. Global warming and thermohaline circulation stability. *Philosophical Transactions of the Royal Society of London Series A-Mathematical Physical and Engineering Sciences* **361**(1810), 1961–1974.

Yohe, G., Schlesinger, M. E. and Andronova, N. G. 2006. Reducing the risk of a collapse of the Atlantic thermohaline circulation. *The Integrated Assessment Journal* **6**(1), 57–73.

Zickfeld, K., Slawig, T. and Rahmstorf, S. 2004. A low-order model for the response of the Atlantic thermohaline circulation to climate change. *Ocean Dynamics* **54**(1), 8–26.

Zickfeld, K., Levermann, A., Morgan, M. G., Kuhlbrodt, T., Rahmstorf, S. and Keith, D. W. 2007. Expert judgements on the response of the Atlantic meridional overturning circulation to climate change. *Climatic Change* **82**, 235–265.

Zickfeld, K., Eby, M. and Weaver, A. J. 2008. Carbon-cycle feedbacks of changes in the Atlantic meridional overturning circulation under future atmospheric CO_2. *Global Biogeochemical Cycles* **22**, GB3024.

Zwally, H. J., Abdalati, W., Herring, T., Larson, K., Saba, J. and Steffen, K. 2002. Surface melt-induced acceleration of Greenland ice-sheet flow. *Science* **297**(5579), 218–222.